Molecular-dynamics study of lattice-defect-nucleated melting in metals using an embedded-atom-method potential

J. F. Lutsko, D. Wolf, S. R. Phillpot, and S. Yip*
Materials Science Division, Argonne National Laboratory, Argonne, Illinois 60439
(Received 20 January 1989)

The high-temperature behavior of a high-angle twist grain boundary, a free surface, and planar arrays of voids of various sizes, all on the (001) plane in copper, are studied through molecular-dynamics simulation using an embedded-atom-method potential. Independently, we determine the thermodynamic melting point, T_m of this potential through an analysis of the free energies of a perfect crystal and the liquid phase. It is found that an ideal crystal consisting of nearly 1000 atoms may be superheated over 200 K above T_m while the introduction of any of the defects listed above nucleates melting at any temperature above T_m. We conclude that nucleation of the liquid phase at extrinsic defects is the most rapid, and therefore the dominant, mechanism of melting.

I. INTRODUCTION

The fundamental concept of melting is based on the coexistence of the solid with the liquid when the free energies of the two phases are equal. It is implied that at temperatures above this coexistence the solid is unstable, but neither the mechanism of melting nor the kinetics of the process are considered in the thermodynamic definition. In reality, melting is observed in the presence of surfaces and over a finite time interval, and despite a wealth of experimental data,[1] it is not clear conceptually how the observed kinetic behavior is to be interpreted in the context of the thermodynamic basis of the transition.

A number of theories of melting have been proposed treating the phenomenon as a homogeneous, bulk process involving either a lattice instability (see, for example, Refs. 2 and 3) or the spontaneous generation of thermal defects (see, for example, Ref. 4). Because these descriptions do not consider the effects of extrinsic defects such as a free surface or an internal interface, it is an open question to what extent they are relevant to the phenomena physically observed. A variety of experimental data now exist which point to the controlling role of an extrinsic surface.[5–11] Several recent measurements demonstrate that when the surface conditions are modified, the melting point can be depressed[8] or the solid can be substantially superheated.[9–11] The implication is that melting is basically a heterogeneous process and the mechanism of nucleation at extrinsic surfaces generally determines the kinetics.

It is conceivable that a study in which the free energies of equilibrium solid and liquid phases are explicitly calculated and the dynamical details of melting initiating at extrinsic defects are examined at the molecular level can contribute to a clarification of the issues raised above. Such an approach can be realized through atomistic simulations using the method of molecular dynamics.[12] Molecular dynamics (MD) and the related method of Monte Carlo[13] have been used successfully to calculate phase diagrams of model systems;[14,15] they also have been used extensively to study melting and freezing phenomena.[16,17] While these are powerful techniques for dealing with the statistical mechanics of a many-body system, their applications to real materials have limitations imposed by the interatomic potential used and the finite system size and time duration of simulation.

Another aspect of molecular dynamics relevant to the present discussion is the determination of the melting point T_m of the simulation model. In principle, for a given potential function adopted for the simulation, free-energy calculations should be performed to determine T_m. If this is not done, then one does not know the true melting point of the model. In some simulations, self-consistency was attempted by determining a temperature T_s where the lattice collapses, and where system properties such as the potential energy and the volume show a stepwise increase. This behavior is the manifestation of the mechanical instability given by the Born criterion.[18] Since T_s can be considerably higher than T_m, any failure to distinguish between these two quantities will result in confusion in interpreting the melting characteristics of the model system.

The advent of many-body potentials[19,20] for metals eliminates several basic objections against the use of conventional pair potentials.[21,22] In particular, it is well known that cubic systems may, and in reality do, possess three independent elastic constants while central-force potentials constrain the number of independent elastic constants to two.[23] This deficiency is intimately connected with the fact that bonding in metals is fundamentally many body in nature. Many-body potentials such as the embedded-atom-method (EAM) potentials are explicitly parameterized to give the correct (experimental) elastic constants and, in total, are fit to at least six experimentally determined parameters. (This should be compared with, for example, the two parameters used to fit a Lennard-Jones potential.) As a result, the EAM potential has proved to be superior to central-force potentials when used in conjunction with computer simulation to calculate physical properties which can be quantitatively compared with experiment.[24,25] For example, the EAM predicts an inward relaxation of the outermost plane at a

free surface of comparable magnitude to that observed in experiment,[26] while most central-force potentials predict an outward relaxation. The EAM potential also has been used in computer simulations to systematically study grain boundaries in both fcc (Ref. 27) and bcc (Ref. 28) metals, elastic properties of grain boundary superlattices,[29] and the high-temperature stability of grain boundaries.[30] In contrast to the free surface, these studies have shown that the EAM potential predicts the same qualitative phenomena in grain boundaries as do central-force potentials.

The purpose of this work is to investigate the role of lattice defects on melting in metals by means of molecular-dynamics simulation using an EAM potential function. As in the companion study of silicon which makes use of a comparably realistic potential function,[31] we study the melting behavior initiated at a grain boundary and a free surface; in addition the effects of voids are also considered. Our simulation results on silicon show that a perfect crystal without a surface can be superheated substantially above its thermodynamic melting point. The lattice does become mechanically unstable at a certain temperature; its precise value can be expected to vary somewhat with the size of the system considered and the way in which it is superheated. When an extrinsic surface is introduced into the crystal, melting at a temperature above the thermodynamic melting point, T_m, clearly initiates at the surface, and the melt propagates into the bulk crystal at a rate that can be adequately followed on the simulation time scale. It is found that extrapolation to zero propagation velocity leads to T_m for both the grain-boundary system and the crystal with a free surface. The implication is that the presence of an extrinsic surface introduces a mechanism for the kinetic process but does not alter the intrinsic (thermodynamic) melting point of the system. As we will show in this paper, the same conclusions are reached in the study of melting behavior in metals.

From the metallurgical standpoint melting at grain boundaries is a process of great importance because of its effects on mechanical properties of solids. There are experimental indications that some kind of structural transition can take place at temperatures distinctly below T_m.[32] On the other hand, measurements carried out specifically to investigate the possibility of a premelting transition[33–35] show that complete grain-boundary melting below T_m, "premelting," in the sense of the boundary being replaced with a liquid layer of several atomic diameters, is not observed. Thermal stability of bicrystal models has been investigated by molecular-dynamics simulations,[36–38] with the results leading to inconsistent interpretations. Two observations have been made recently which should help to clarify the situation, one dealing with the effects of grain-boundary (GB) migration on local disordering[39] and the other concerning the importance of a proper determination of T_m for the simulation model system.[30] In our results on silicon where GB migration does not occur, we observe no indications of grain-boundary premelting.[31,40] In the case of metals, GB migration can be readily activated at temperatures well below T_m, but here also we do not find premelting up to the highest temperature below T_m studied (about $0.9T_m$).

In contrast to grain boundaries, premelting on a metal surface has been observed by backscattering measurements on Pb,[41] the process occurring at approximately $0.75T_m$. The data provide support for the theoretical prediction that the thickness of the surface-melt layer should diverge logarithmically as T_m is approached.[42] Simulation studies of surface disordering and melting have been carried out on various model systems.[43–46] In the case of metals, disordering below T_m on aluminum surfaces has been observed recently,[45] but no studies at temperatures above T_m have been reported.

The plan of this paper is as follows. In the next section, we discuss the EAM potential used in the present study. In Sec. III, the details of the free-energy analysis used to determine the thermodynamic melting point of this potential are described. Section IV contains the details of the methods used in the simulation of defected systems including a description of the bicrystal program used. Sections V–VII contain the results of superheating a grain boundary, a free surface, and various-sized voids. Finally, in Sec. VIII, we discuss the implications of our results on the question of the microscopic mechanism of melting.

II. INTERATOMIC POTENTIAL

As discussed in the Introduction, the majority of prior simulations, including almost all studies of melting-related phenomena in metals, have been performed using central-force potentials. A serious deficiency of these potentials is that they poorly represent atomic bonding in a metal. Metallic bonding has long been understood to arise from the interaction of individual atoms with the electron gas, or Fermi sea, of the metal. Because the local electron density depends on the local arrangement of atoms, this bonding depends strongly on the local atomic density in the vicinity of an atom. The embedded-atom method[19,20] is an attempt to model this dependence of the atomic interactions on the local environment. In this sense, the EAM potentials currently provide the most realistic description of interatomic interactions in metals. Indeed, the EAM has met with considerable success in describing such properties as the behavior of surfaces including surface reconstruction, point-defect properties in pure metals, and surface segregation.[24]

The EAM potential is a sum of two terms and is usually written as

$$V=\sum_{j\neq i}\Phi(q_{ij})+\sum_i F_i(\rho_i^T)\ , \tag{1}$$

where $\mathbf{q}_i$ is the position of the ith atom and q_{ij} is the distance between atoms i and j. The first term on the right-hand side in Eq. (1) represents the screened Coulombic repulsion of the ion cores and is a sum, therefore, of pairwise interactions. The second term is many-body in nature and represents the embedding of the ion cores in the electron gas. The function $F_i(\rho_i^T)$ is termed the embedding function. The total charge density experienced by atom i, ρ_i^T, is the sum of the charge densities at the posi-

tion $\mathbf{q}_i$ of all atoms except atom i:

$$\rho_i^T = \sum_{j \neq i} \rho_j(q_{ij}) \ . \tag{2}$$

In practice, the atomic-charge densities are approximated as the isolated atomic-charge distributions as opposed to the true charge distributions that would result from a self-consistent first-principles calculation. The embedding function is determined by the universal binding function of Rose *et al.* and the free parameters in the repulsive term are fitted to various bulk properties (see, i.e., Ref. 24).

The EAM potential used in the present work was parameterized to describe copper in the context of copper-nickel alloys. Also, the pair potential and the charge densities were cut off at $r_c = 1.35a_0$, where a_0 is the zero-temperature lattice parameter. These functions were then shifted so as to go smoothly to zero at r_c. For example, the shifted charge densities, $\rho_i^s(r)$, are related to the unshifted functions, $\rho_i(r)$, by

$$\rho_i^s(r) = \rho_i(r) - \rho_i(r_c) - (r - r_c) d\rho_i(r)/dr|_{r_c} \ . \tag{3}$$

That the shifted functions and their first derivatives go smoothly to zero at the cutoff is particularly important in the study of melting. Otherwise, were the first derivative of the potential not continuous at r_c, atoms in the liquid state which are constantly passing in and out of the cutoff range of other atoms would experience discontinuous forces. For later reference, we note that the equilibrium lattice parameter at zero temperature is $a_0 = 3.6208$ Å, and the cohesive energy in the ideal crystal at zero temperature is $-3.430\,937$ eV/atom.

Due to the shifting of the potential and the fact that the potential used was not parametrized to elemental copper (but copper-nickel alloys, instead), we will see below that the melting point differs from the experimental melting point of copper. However, as we are interested in generic phenomena, and not in predicing experimental results, this is not a limitation. We feel that our results will be representative of all fcc metals.

III. THERMODYNAMIC MELTING POINT

In this section, we describe the determination at constant (zero) pressure of the thermodynamic melting point, T_m, defined as the temperature at which the Gibbs free energy per atom of the solid, $g_{\text{solid}}(T)$, and that of the liquid, $g_{\text{liquid}}(T)$, are equal:

$$g_{\text{solid}}(T_m) = g_{\text{liquid}}(T_m) \ . \tag{4}$$

(Throughout this section, we will use lower-case symbols to denote thermodynamic quantities divided by the number of atoms.) As discussed in the Introduction, T_m may be considerably lower than the temperature at which the crystal spontaneously melts, T_s. Therefore, to accurately determine T_m we must determine the liquid and solid free energies as a function of temperature and thus explicitly determine T_m from Eq. (4). The procedures used follow closely those described in Refs. 15 and 43.

A. Simulation procedures

All simulations to be described in this subsection were performed using periodic-border conditions in the x, y, and z directions of the (cubic) simulation cell [we shall call this border condition three-dimensional (3D) PBC's]. The systems, consisting of 108 particles, were equilibrated for approximately 1000 time steps (1 time step ~ 0.002 ps) at the desired temperature, which was maintained by rescaling the velocities in every time step. Statistics were then collected while the Nosé thermostat[47] was used to simulate a canonical ensemble. The lattice parameters for each temperature were determined using the Parrinello-Rahman constant-pressure method[48] in the solid-state simulations while the Andersen constant-pressure method[49] was used in the liquid-state simulations. This is because the Parrinello-Rahman scheme allows strain fluctuations against which the liquid is unstable. All other properties were determined from constant-volume simulations. Second-order polynomial fits to the lattice parameter as a function of temperature are given in Table I.

B. Free energy in the solid state

The Gibbs free energy per particle at zero pressure, $g(T,P=0)$, is related to the internal energy per particle, $u(T,P=0)$, and the specific entropy, $s(T,P=0)$, by the thermodynamic relation[50]

$$g(T,P=0) = u(T,P=0) - Ts(T,P=0) \ . \tag{5}$$

The entropy can be eliminated from Eq. (5) by expressing it in terms of the Gibbs free energy using the standard thermodynamic relation:[50]

$$s(T,P=0) = -\partial g(T,P=0)/\partial T|_{P=0} \ . \tag{6}$$

Substituting Eq. (6) into Eq. (5) yields a differential equation for the Gibbs free energy in terms of the internal energy. Upon solving this equation, one obtains an expression, valid for any system, for the difference in the Gibbs free energy at different temperatures

$$g(T,P=0)/T = g(T_0,P=0)/T_0 - T\int^T d\tau\, u(\tau,P=0)/\tau^2 \ . \tag{7}$$

Equation (7) is the fundamental equation we will use in determining the free energy as a function of temperature. It expresses the temperature dependence of the free energy in terms of that of the internal energy—a quantity

TABLE I. Coefficients α,β,γ, of a second-order polynomial fit to the lattice parameter in the solid, $a_s(T)$, and the liquid, $a_l(T)$, as a function of temperature: $a_s(T) = \alpha + \beta T + \gamma T^2$. Lattice parameters are in units of a_0 and temperatures are in units of 1000 K. The "lattice parameter" in the liquid is obtained from the cube root of the volume.

Coefficient	$a_s(T)$	$a_l(T)$
α	1.0000	0.9922
β	0.015 45	0.0400
γ	0.005 159	0.0000

which is easily and reliably obtained from simulation.

In order to use Eq. (7), it remains to determine the absolute free energy at some temperature, T_0. However, rather than directly determining $g_{\text{solid}}(T_0,P)$, we consider the difference in free energy $\delta g(T,P)$ of the perfect solid and the same system in the harmonic approximation

$$\delta g(T,P=0)/T=\delta g(T_0,P=0)/T_0 - \int^T d\tau\, \delta u(\tau,P=0)/\tau^2 , \quad (8)$$

where $\delta u(T,P=0)$ is the difference between the internal energy of the fully interacting solid, $u_{\text{solid}}(T,P=0)$, and the harmonic reference system, $u_{\text{har}}(T,P=0)$. For a classical system at low temperatures[50] $\delta g(T_0,P=0)\propto T_0^2$ so we can take the zero-temperature limit of Eq. (8). Upon rearrangement, this yields

$$g_{\text{solid}}(T,P=0)=g_{\text{har}}(T,P=0) - T\int^T d\tau\, \delta u(\tau,P=0)/\tau^2 , \quad (9a)$$

where

$$\delta u(T,P=0)=u_{\text{solid}}(T,P=0)-3k_BT(N-1)/N-\phi_0 . \quad (9b)$$

Here, N is the number of atoms, k_B is Boltzmann constant, and $\phi_0=u_{\text{solid}}(T=0,P=0)$ is the potential energy per particle in the static (zero-temperature) lattice with the original potential. The factor $(N-1)$ occurs because the center of mass is fixed in our simulations, since the systems are conservative, and there are, therefore, only $N-1$ degrees of freedom. This technique, using the harmonic reference system to avoid lengthy MD simulations which would otherwise be necessary to determine $g_{\text{solid}}(T_0,P=0)$, was first described by Broughton and Li.[15]

We have performed simulations of the 108-particle perfect crystal at ten different temperatures ranging from 200 to 1400 K and determined $u_{\text{solid}}(T,0)$ at each temperature. (The upper limit of 1400 K was chosen because the crystal spontaneously melts above this temperature. This is discussed in greater detail in the following section.) After 10 000 time steps, the time average of $u_{\text{solid}}(T,0)$ at each temperature showed fluctuations of less than 0.01% which we take as the errors in these numbers. Table II gives a second-order polynomial fit to $\delta u(T,P=0)/T^2$. The expression for $g_{\text{har}}(T,P=0)$ is given in the Appendix. The result of an evaluation of that expression yields, for our system,

$$g_{\text{har}}(T,P=0)=\phi_0-0.3888T-0.2585T\ln(T) , \quad (10)$$

where g_{har} is in units of eV, the temperature is in units of 1000 K, and $\phi_0=-3.430\,937$ eV represents the zero-temperature cohesive energy given in Sec. II. Equations (8)–(10) and Table II completely characterize the free energy of the perfect solid as a function of temperature. Because $u_{\text{solid}}(T)$ was determined from $T=0$ K to $T=1400$ K, we expect the values of $g_{\text{solid}}(T)$ determined by this method to be accurate over the same range of temperatures.

TABLE II. Coefficients of a second-order polynomial fit to the difference between the solid and harmonic internal energies divided by the squared temperature, $\delta u_s(T)/T^2$, and the liquid internal energy divided by the squared temperature, $u_l(T)/T^2$, as functions of temperature: $\delta u_s(T)/T^2=\alpha+\beta T+\gamma T^2$. Energy is in units of eV and temperature is in units of 1000 K.

Coefficient	$\delta u_s(T)/T^2$	$u_l(T)/T^2$
α	0.014 410	−8.036
β	−0.001 956	6.933
γ	0.005 436	−1.660

C. Liquid-state free energy

To determine $g_{\text{liquid}}(T,P=0)$, we begin again with Eq. (7). The internal energy of the liquid was determined at ten different temperatures from 1350 to 1800 K. The liquid was first created by equilibrating the 108-particle system at 2500 K for 20 000 time steps. The temperature was then stepped down 100 K every 10 000 time steps until a temperature of 1800 K was achieved. The internal energy was then determined at ten temperatures ranging from 1800 to 1350 K following the same procedure, and with comparable accuracy, as in the case of the solid. Table II also gives a second-order polynomial fit to $u_{\text{liquid}}(T,P=0)/T^2$.

To determine $g_{\text{liquid}}(T_0,P=0)$ we, again, need a convenient reference system. The only fluid system for which it is possible to analytically calculate the free energy is the ideal gas. This can indeed be used as a reference by first noting that at zero pressure, the Gibbs free energy is equal to the Helmholtz free energy,[50] $a(T,V)$, evaluated at $V=V(T,P=0)$. The variation of the Helmholtz free energy with respect to volume, while holding temperature constant, is given by

$$da(T_0,V)=-(1/N)P(T_0,V)dV , \quad (11)$$

so that, upon integration along an isotherm,

$$a(T_0,V)=a(T_0,V_0)-(1/N)\int^V dv\, P(T_0,v) . \quad (12)$$

The same expression holds for an ideal gas. Denoting the difference in the Helmoltz free energy of the liquid and the ideal gas by $\delta a(T,V)$, we have that

$$\delta a(T_0,V)=\delta a(T_0,V_0)-(1/N)\int^V dv\, \delta P(T_0,v) =\delta a(T_0,V_0)+\int^n dn\, \delta P(T_0,n)/n^2 , \quad (13)$$

where $\delta P(T_0,v)$ is the difference in pressure between the liquid and the ideal gas. Notice that we have changed variables in the integration from volume to number density, n. As the volume becomes infinite (or the density goes to zero) the liquid becomes a noninteracting ideal gas so that $\delta a(T,V_0)$ becomes zero and we have

$$a_{\text{liquid}}(T_0,V)=a_i(T_0,V)+\int^n dn\, \delta P(T_0,n)/n^2 , \quad (14)$$

where $a_i(T_0,V)$ is the ideal-gas free energy. Unfortunately, this expression cannot be usefully evaluated by simulation because the liquid undergoes a phase transformation

to a gas as the volume is expanded. The pressure is therefore not a continuous function and the numerical integration of Eq. (14) cannot be performed accurately.

The liquid-gas phase transition can be circumvented by first modifying the potential. We replace the EAM potential V with a new potential V_λ given by

$$V_\lambda = \sum_{i \neq j} \Phi(q_{ij}) + \lambda \sum_i F_i(\rho_i^T) \ . \tag{15}$$

When λ is unity, V_λ represents the original Cu potential, whereas when λ is zero the potential is purely repulsive. The purely repulsive system is useful because no phase transition occurs as the volume increases.[43] Its free energy, $a_{\rm rep}(T,V)$, may therefore be computed using Eq. (14), i.e., by expanding the system towards the ideal-gas, infinite-volume limit. The free energy of the original liquid is then related to that of the purely repulsive liquid by[43]

$$a_{\rm liquid}(T,V) = a_{\rm rep}(T,V) + \int^1 d\lambda \langle (1/N) \sum_i F_i(\rho_i^T) \rangle_\lambda \ , \tag{16}$$

where the integrand in Eq. (16) is simply the average value of the embedding function when the potential given by Eq. (15) is used.

The calculation of $a_{\rm liquid}(T_0,V)$ thus consists of three steps. The first is to determine the integrand of Eq. (16) for several values of λ and to numerically evaluate Eq. (16). At this point, the liquid is purely repulsive. The second step is to expand the system and to determine the pressure as a function of density at several different points. These data are used to numerically evaluate Eq. (14) in which $a_{\rm liquid}(T,V)$ is replaced by $a_{\rm rep}(T,V)$. The final step is to analytically evaluate the ideal-gas free energy $a_i(T,V)$.

We have carried out this procedure at a temperature of $T_0 = 1800$ K. The integrand in Eq. (16) was evaluated at five values of λ between 0 and 1. A second-order polynomial fit to these data is given in Table III. After 10 000 time steps at each value of λ, the average of the embedding function converged to four significant figures. By using various polynomial fits to evaluate Eq. (16), we find that

$$a_{\rm liquid}(T_0,V) = a_{\rm rep}(T_0,V) - 4.439 \pm 0.001 \text{ eV} \ . \tag{17}$$

The pressure of the purely repulsive liquid was evaluated for ten values of the density from $n = 3.321$ atoms/a_0^3 (the density of the Cu liquid at 1800 K and zero pressure) to $n = 0.300$ atoms/a_0^3. At the higher densities, simulations of 10 000 time steps yielded convergence of the pressure to 0.01%. At the lower densities, however, there are fewer collisions and the statistics become poorer. Therefore, the length of the simulations was increased by a factor of 4 in order to yield similar accuracy. A second-order polynomial fit of $\delta P(T,n)/n^2$ is given in Table III, where the second virial coefficient was used to provide an additional point at zero density. From various such polynomial fits we estimate that

$$a_{\rm rep}(T_0,V) = a_i(T_0,V) + 1.8694 \pm 0.002 \text{ eV} \tag{18}$$

TABLE III. Coefficients of second-order polynomial fit to the average of the embedding function, $\langle F \rangle_\lambda$, as a function of λ and of $\delta P(n)/n^2$ as a function of density: $\langle F \rangle_\lambda = \alpha + \beta\lambda + \gamma\lambda^2$ and $\delta P(n)/n^2 = \alpha + \beta n + \gamma n^2$. Energy is in units of eV and length is in units of a_0.

Coefficient	$\langle F \rangle_\lambda$	$\delta P(n)/n^2$
α	−4.395	0.1699
β	−0.3605	0.1132
γ	−0.077 23	0.055 70

at $T = 1800$ K. Finally, $a_i(T_0,V)$ is calculated to be -1.947 eV at $T_0 = 1800$ K and $n = 3.321$ atoms/a_0^3 (see the Appendix for details). Combining Eqs. (17) and (18) we have that

$$g_{\rm liquid}(T_0 = 1800 \text{ K}, P = 0) = -4.517 \pm 0.003 \text{ eV} \ . \tag{19}$$

Equations (19) and (7) and $u_l(T, P = 0)$ as given in Table II completely specify the liquid free energy as a function of temperature. This method of determining the free energy of the liquid is identical to that used by Broughton *et al.*[15,43]

D. Thermodynamic melting point

The thermodynamic melting point T_m is determined by equating the liquid and solid free energies. By using various polynomial fits to the MD data and taking into account the known errors, we estimate T_m for our system to be 1171±30 K. Figure 1 shows the solid-phase and liquid-phase free energies as a function of temperature near T_m. In fact, the error in this value may be somewhat larger than indicated. The reason for this is that the liquid free energy is extrapolated from a value determined at 1800 K and the absolute value of the liquid free energy undoubtedly becomes less reliable the further one extrapolates away from this value. This source of error could be reduced by redetermining $g_{\rm liquid}(T_0, P = 0)$ at a lower value of T_0. In addition, $u_{\rm liquid}(T)$ was necessarily extrapolated below temperatures at which it had been ex-

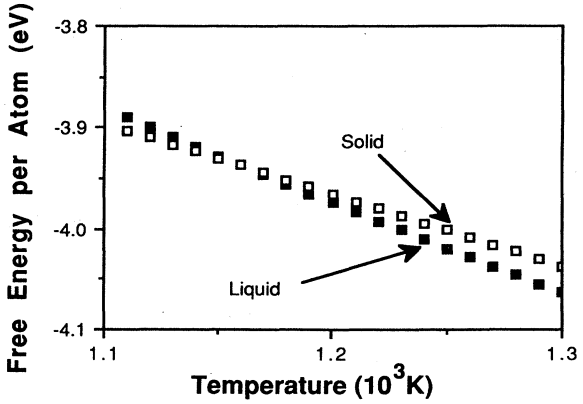

FIG. 1. Free energy of the solid phase (open symbols) and the liquid phase (solid symbols) as a function of temperature near the melting point.

plicitly determined from simulation. We do not consider this to be a serious source of error since the internal energy is expected to be a smooth function of temperature. Finally, we note that T_m as determined here is significantly lower than the experimentally determined melting point for copper ($T_{m,\text{expt}} \sim 1350$ K). This is because (a) the potential was not parameterized to elemental copper and (b) the potential was shifted as described in Sec. II. In practice, when the elemental potential is used the temperature scales at which various phenomena occur are shifted up about 100 K relative to the potential used here, in better agreement with experiment.

IV. SIMULATION METHODS FOR DEFECTED SYSTEMS

In this section, we describe several aspects of our methods for the simulation of defect-induced melting which are essential for the appreciation of the results to be presented. These include the use of a recently developed bicrystal simulation model and the methods of data analysis used to monitor the local order in the system. In the following sections, the results of simulations of three types of defects, a grain boundary, a free surface, and various sized voids, will be discussed. For clarity in the discussion of the results, the different considerations which enter into the method of simulation of each system will be described here.

A. Bicrystal simulation method

In simulation studies of interfaces a technical problem arises in the implementation of border conditions on the simulation cell which properly represent the effects of the medium beyond the cell. As long as the interface is planar and coherent, i.e., as long as it can be characterized by a periodic planar unit cell, 2D periodic borders (2D PBC's) are appropriate in the plane of the interface (what we shall call the x-y plane, see Fig. 2). However, perpendicular to the interface, i.e., in the z direction, the system is inhomogeneous and the imposition of periodic borders in this direction (i.e., the use of 3D PBC's) gives rise to a second interface in the simulation cell. Recently a new border condition has been proposed which introduces moveable perfect-crystal blocks at the two ends of the simulation cell in the z direction.[51] This model allows the simulation of isolated interfaces embedded in otherwise perfect crystal. The present simulation makes use of this 2D PBC model.[51]

Figure 2 shows the simulation cell consisting of a region I in which atoms move according to Newtonian equations of motion and a region II which consists of two rigid blocks of atoms. The simulation cell is periodic in the x and y directions. The extent of the rigid blocks in the z direction is determined by the range (i.e., the cutoff radius) of the potential. Initially, the positions of the rigid blocks are fixed by taking the distance between the outermost plane of region I and the first plane of region II to be the perfect-crystal interplanar spacing. Such a region I–region II strategy is commonly used in zero-temperature (lattice statics) simulations of grain boundaries.

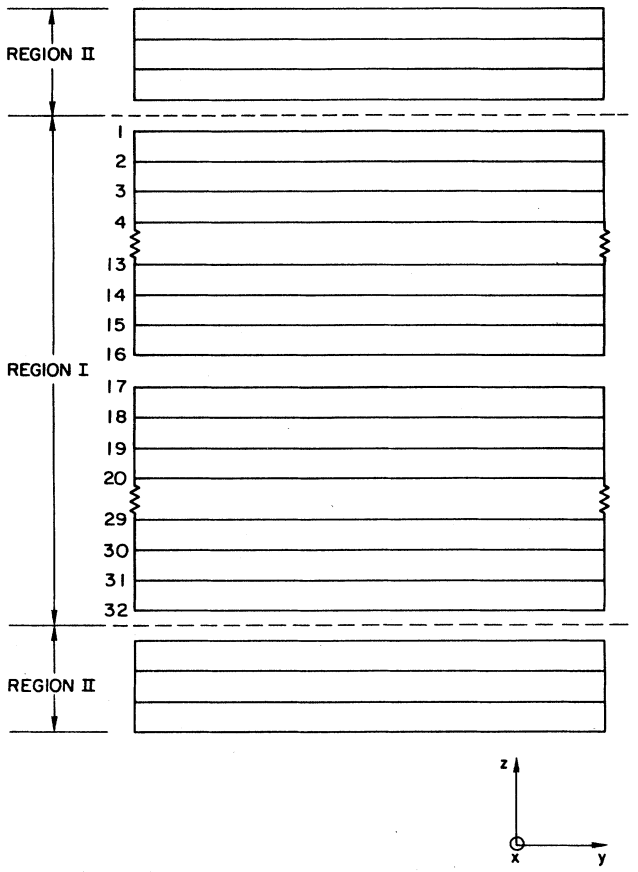

FIG. 2. Schematic of our simulation cell. Region I contains 32 planes with 29 atoms in each plane. Initially, the GB lies between planes 16 and 17.

The new border conditions specify how the rigid blocks move during the simulation. Each rigid block is allowed to move as a unit parallel to the interface in response to the total force exerted on it by the atoms in region I. In addition, a restricted Parrinello-Rahman constant-pressure scheme[48] is used to allow the length of the simulation cell in the z direction to fluctuate in response to the pressure in region I. The dimensions of the simulation cell in the plane of the interface are fixed by the semi-infinite bulk regions the interface is embedded in; they are, therefore, determined by the lattice parameter of the ideal crystal at the simulation temperature. This lattice parameter is determined from an independent simulation of an ideal crystal with 3D PBC's at the desired temperature. Further details are given in Ref. 51.

B. Free-surface simulation

The simulation of a free surface on a bulk substrate may be treated within the framework of the bicrystal simulation model described above by the removal of either one or both of the region-II rigid blocks. The removal of one block would correspond to the simulation of a free surface on a bulk substrate. This method has been used in many simulation studies of free surfaces.[45,46] Since the greatest pressure fluctuations are expected to take place near the free surface, which is free to respond

to them, it is inappropriate in this case to use the Parrinello-Rahman constant-pressure scheme.

In our simulations, we have chosen to remove both rigid blocks thus creating a thin-slab geometry. The advantage of this is that, with two free surfaces present, we gain twice as much data as we would if we only removed one rigid block. In order to simulate free surfaces on a bulk substrate, we continue to hold fixed the lattice parameter in the x-y plane of the thin slab at the value appropriate for a bulk ideal crystal. Provided the surfaces are far enough apart that they do not interact, we then expect each free surface to behave as if it were attached to a bulk substrate. In the simulations described in Sec. VI, the free surfaces are initially nearly 60 Å apart and the energy and surface relaxation indicate that the surfaces do not interact. The interaction of the two liquid-solid interfaces which exist after the surfaces melt will be discussed in Sec. VI.

C. Void simulation

The bicrystal simulation model has also been used in the simulation of small voids to be discussed in Sec. VII. In this case, the region I–region II geometry was used even though region I contained no interface. This allows us to simulate a periodic planar array of voids (periodic due to the periodicity in the x-y plane) by removing atoms from the center of region I to create a single void in the simulation cell. Such a system bears an obvious analogy to a grain boundary (both are more or less planar, periodic defects) with the additional degree of freedom of controlling the amount of disorder introduced by the defect simply by varying the size of the void.

D. Equilibration procedure and superheating

We find that the degree to which an ideal crystal may be superheated in a computer simulation depends strongly on the size of the system and the equilibration procedure (i.e., the method by which the temperature is varied and maintained). Because we are interested in comparing different possible mechanisms of melting, a single equilibration procedure has been used in all simulations. In addition, the size and geometry of the various systems are chosen to be as similar as possible.

The systems were initially instantaneously raised to a temperature of 600 K which was maintained for 1000 time steps. The time step used in all simulations was approximately 0.002 ps, which provided energy conservation at constant volume to six significant figures over an interval of 1000 time steps. Because we are interested in studying the melting transition, which requires a latent heat, the velocities of the atoms were rescaled after every time step so as to maintain a constant temperature. This thermostating, which provides a crude approximation to a canonical ensemble, acts as a thermal reservoir allowing the system to give up or absorb energy as needed.

After the equilibration at 600 K, the temperature was raised 100 K every 200 time steps until the temperature reached 1000 K. This temperature was maintained for 1000 time steps to allow at least partial equilibration. Following this, the temperature was then raised 100 K every 1000 time steps until the desired temperature was reached. With this equilibration procedure, we were able to superheat an ideal crystal using the region I–region II simulation method to between 1400 K, where the crystal was stable, and 1500 K, where the crystal spontaneously melted. Therefore, all simulations to be discussed below were in the range from 1100 to 1400 K. The limit to superheating that we were able to obtain will be discussed in Sec. VIII in the context of the Born criterion,[18] which gives an upper limit to superheating.

E. Characterization of planar disorder and melting

The detailed information obtained from MD simulations is commonly condensed into standard thermodynamic and structural quantities. However, as we are interested in the present study in monitoring the thermal disorder associated with essentially planar defects, it is important to monitor the spatial variations of the relevant properties in the direction perpendicular to the plane of the defects. To obtain such information, we divide region I into slices along the z direction. The widths of the slices are chosen so that each slice contains, initially, one lattice plane. Properties such as the internal energy and mean-square displacement (MSD) were then monitored in each slice.

To investigate the breakdown of crystalline order upon melting, we define the squared magnitude of the static structure factor, $S(\mathbf{k})$, which for brevity we denote simply as $S^2(\mathbf{k})$,

$$S^2(\mathbf{k}) = \left[1/N \sum_i \cos(\mathbf{k}\cdot\mathbf{q}_i)\right]^2 + \left[1/N \sum_i \sin(\mathbf{k}\cdot\mathbf{q}_i)\right]^2 , \tag{20}$$

where $\mathbf{q}_i$ is the position of atom i. For the overall $S^2(\mathbf{k})$, all atoms in the simulation cell are included in the sums in Eq. (20), whereas for the planar structure factor, $S_p^2(\mathbf{k})$, only atoms in a given lattice plane are considered. For an ideal-crystal lattice at zero temperature, $S_p^2(\mathbf{k})$ then equals unity for any wave vector $\mathbf{k}$ which is a reciprocal lattice vector in that plane. By contrast, in the liquid state (without long-range order in the plane) $S_p^2(\mathbf{k})$ fluctuates near zero.

In the case of a GB, the two halves of the bicrystal are rotated relative to one another. Therefore, a reciprocal-lattice vector in one-half of the bicrystal is not a reciprocal-lattice vector in the other half. Thus, two different wave vectors are required to monitor planar order in the two halves. We shall call these wave vectors $\mathbf{k}_1$ and $\mathbf{k}_2$. They are related by the relative rotation of the two halves of the bicrystal. For a well-defined lattice plane, say in crystal 1, $S_p^2(\mathbf{k}_1)$ then fluctuates near a finite value (<1) appropriate for the temperature of the crystal, whereas $S_p^2(\mathbf{k}_2)$ fluctuates near zero. In the interface region, due to local disorder, one expects somewhat lower values of $S_p^2(\mathbf{k}_1)$. By monitoring $S_p^2(\mathbf{k}_1)$ and $S_p^2(\mathbf{k}_2)$, every plane may be characterized as (a) belonging to crystal 1 [for $S_p^2(\mathbf{k}_1)$ finite, $S_p^2(\mathbf{k}_2)$ near zero], (b) belonging to crystal 2 [for $S_p^2(\mathbf{k}_1)$ near zero, $S_p^2(\mathbf{k}_2)$ finite], or (c) disordered [for $S_p^2(\mathbf{k}_1)$ and $S_p^2(\mathbf{k}_2)$ near zero]. The vectors $\mathbf{k}_1$ and $\mathbf{k}_2$ were chosen, in the present case, to be reciprocal-lattice

vectors in the ⟨100⟩ direction.

As a further measure of the overall disorder in the system, we introduce a quantity $N_{\rm def}$ which is a measure of the number of "defected" atoms in the system. To determine whether or not an atom is defected, we first define a distance $r_{\rm def}$ which in our case is taken to be halfway between the first- and second-nearest-neighbor shells in the ideal-crystal lattice (with the lattice parameter appropriate for the temperature of the crystal). An atom, say atom n, is then classified as defected if the number of atoms k within a sphere of radius $r_{\rm def}$ is not equal to the number in the ideal-crystal lattice (i.e., if the local density near atom n differs from that in the perfect lattice). For our choice of $r_{\rm def}$, k is the number of nearest neighbors in the perfect lattice. Because of the change in density in going from the solid state to the liquid state, an atom in the liquid is, usually, characterized as defected. On the other hand, $r_{\rm def}$ is large compared to the amplitude of atomic vibration in the perfect crystal, even at high temperatures, so an atom in the solid is classified as not defected.

V. GRAIN-BOUNDARY NUCLEATED MELTING

A. Grain-boundary geometry

The grain boundary chosen for the present study is the so-called Σ29 (001) symmetrical twist boundary. This GB, on the (001) plane, is obtained by rotating one perfect semicrystal relative to another by an angle of 43.60° about the (001) plane normal. The system is oriented, as indicated in Fig. 2, with the (001) planar normal along the z axis and, consequently, the x-y plane is parallel to the GB plane. The principal ⟨001⟩ axes of each semicrystal are rotated by 21.80° relative to the x-y axes of the simulation cell.

Because of the interface there is no periodicity in the z direction. However, in the x-y plane, the structure is periodic possessing a square-planar repeat unit with an area which is $\Sigma=29$ that of the corresponding primitive planar unit cell ($\Sigma=1$) on the (001) plane in a perfect single crystal. Prior to the finite-temperature simulations, the GB was relaxed at zero temperature and zero pressure to its minimum-energy configuration. The resulting geometry used in the simulations consisted of 32 (001) planes containing 29 atoms per plane for a total of 928 atoms. The dimensions of the simulation cell at zero temperature are $3.808a_0$, $3.808a_0$, and $16.08a_0$ in the x, y, and z directions, respectively, and the GB energy is[27] 710.7 ergs/cm^2.

The primary considerations underlying the choice of this GB are (a) its relatively large planar unit cell and (b) the large spacing of the (001) planes; (the spacing d_0 is $d_0=0.5a_0$ at zero temperature). Because of the large interplanar spacing, the lattice planes are easily distinguished thus making clear the onset of disorder associated with melting. The large planar unit cell allows us to consider this a "generic" high-angle GB as opposed to boundaries with small planar unit cells for which the energy is known to be highly, and unusually, sensitive to translations.[52] Similarly, we choose a *twist* rather than a *tilt* boundary because the symmetrical tilt boundary on a given lattice plane has the smallest planar unit cell of all GB's on that plane and, hence, is also highly sensitive to translations.[52]

B. Simulation results

Shown in Figs. 3(a) and 3(b) are the profiles of the planar structure factor after the GB has been equilibrated at 1100 K for 1000 and over 16 000 time steps, respectively. The profiles are remarkably similar aside from the fact that the position of the GB, as determined from the crossing of $S_p^2(\mathbf{k}_1)$ and $S_p^2(\mathbf{k}_2)$, has shifted. This thermally activated GB migration has been discussed previously.[30,39] However, for the present study we simply observe that at this temperature (about 94% T_m), the grain boundary is completely stable and sharply defined. Other properties such as the plane-by-plane profile of potential energy and MSD are similarly sharp and also indicate that the GB is stable with respect to a spontaneous disordering transition.

Figures 4(a) and 4(b) show the profile of the structure factor after 5000 and 10 000 time steps, respectively, at 1300 K. In contrast to the behavior at 1100 K, a region of disorder forms at the GB and spreads rapidly away from it. It is interesting to note that, from the structure

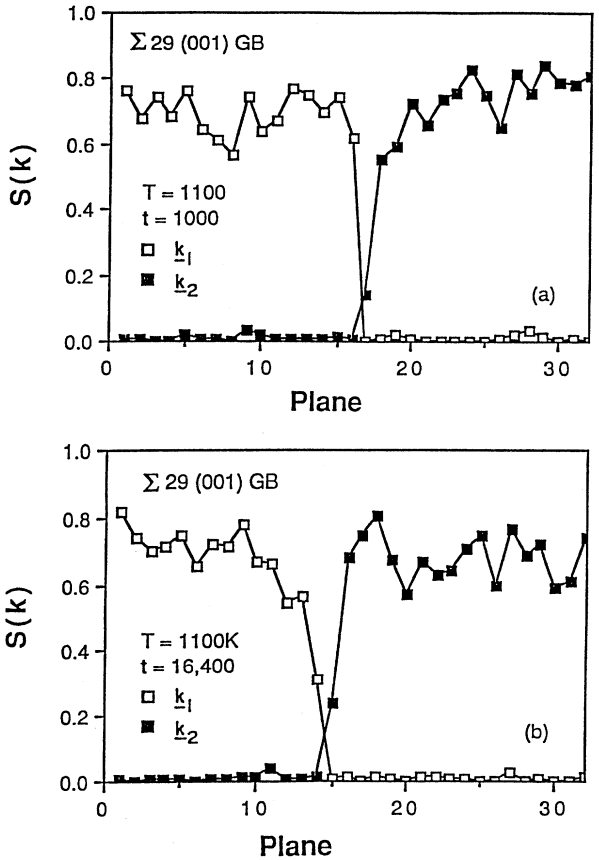

FIG. 3. Instantaneous values of $S_p^2(\mathbf{k}_1)$ and $S_p^2(\mathbf{k}_2)$ for the 32 slices parallel to the (001) Σ29 GB after 1000 [panel (a)] and 16 400 [panel (b)] time steps at 1100 K.

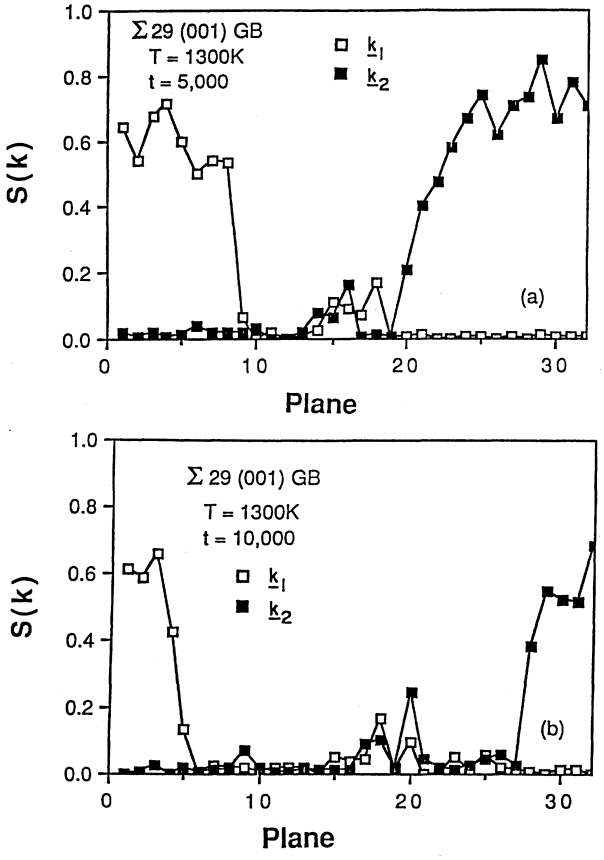

FIG. 4. Instantaneous values of $S_P^2(\mathbf{k}_1)$ and $S_P^2(\mathbf{k}_2)$ for the 32 slices parallel to the (001) Σ29 GB after 5000 [panel (a)] and 10000 [panel (b)] time steps at 1300 K.

factor profiles, the widths of the liquid-solid interfaces appear to be only about two atomic planes in contrast to a GB width, at 1100 K, of about four planes. Figure 5 shows the instantaneous MSD, averaged over planes 15–18, about 116 atoms, as a function of time over the final 10000 time steps of the simulation. The MSD increases nearly linearly, and from its slope a diffusion costant of 4×10^{-9} m^2/s is calculated. This is of the correct order of magnitude for a metal in the liquid state and leads us to conclude that the spreading disorder is a result of melting nucleated at the GB.

The growing liquid region may also be detected by examination of the number of defected atoms. Figure 6 shows N_{def} as a function of time for the GB at 1200, 1300, and 1400 K. In all cases, the number of defected atoms is seen to increase linearly until the liquid-solid interface begins to interact with region II. Because region II consists of rigid blocks of atoms which do not move relative to one another, it cannot melt. Therefore, as the liquid-solid interface approaches region II the rate of melting slows. Figure 7 shows a fit of N_{def} to a linear function of time. In this fit only the points corresponding to $N_{\text{def}} < 800$ have been used to eliminate the data affected by region II. As the figure shows, the rate of increase of N_{def} is, indeed, remarkably linear indicating a constant rate of propagation of the two liquid-solid interfaces.

Figure 6 indicates that the 1400-K system is completely melted after about 15000 time steps. Further evidence that the disordered region is truly liquid is the volume expansion that accompanies it. Because the dimensions of the simulation cell in the x and y directions are held fixed, all volume expansion must be accommodated by a change of the length of the simulation cell (i.e., region I) in the z direction. Shown in Fig. 8 is the length of the simulation cell as a function of time for the GB at 1400 K. It is clear that the volume expansion levels off after about 7000 time steps. From Table I, giving the thermal expansion of the liquid and solid states as a function of temperature, we calculate that the length of the simulation cell in the z direction at 1400 K should be $17.31a_0$ when the system is completely melted. The value obtained by averaging over the last 3000 time steps of the 1400-K simulation is $17.27a_0$ in close agreement with the liquid value. (The small difference is most likely due to incomplete melting at the region I–region II interface.) It is thus quite clear that what is being observed is, indeed, thermodynamic melting.

The velocity of melting may be extracted from the rate of increase of N_{def} by assuming that (a) the liquid-solid interface is planar and that (b) an increase of N_{def} by 58 atoms corresponds to each liquid-solid interface propaga-

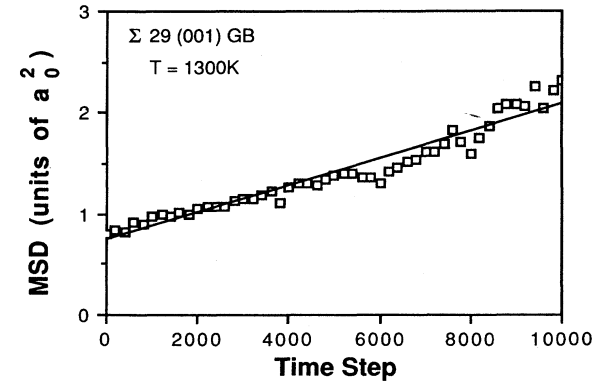

FIG. 5. Instantaneous mean-square displacement averaged over four slices in the disordered region as a function of time.

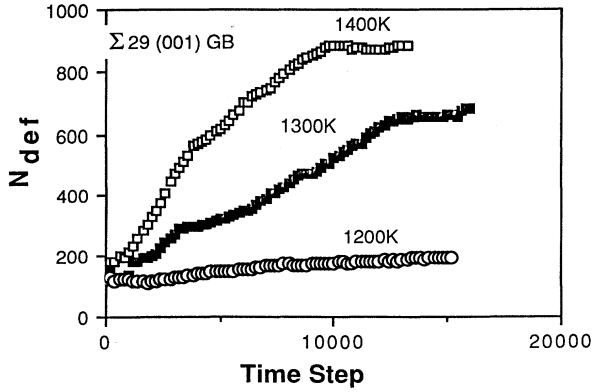

FIG. 6. Number of defected atoms as a function of time for the GB at 1200, 1300, and 1400 K.

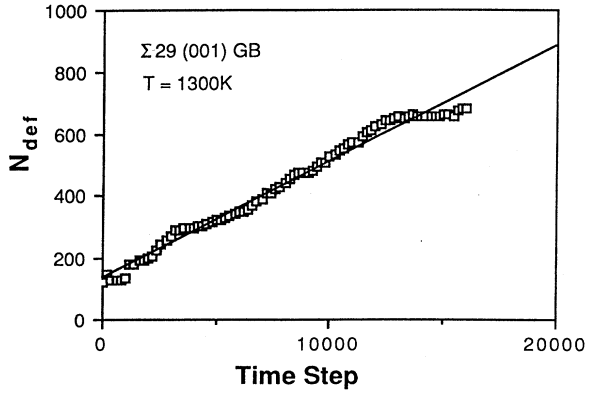

FIG. 7. Fit of $N_{\rm def}$ to a linear function of time.

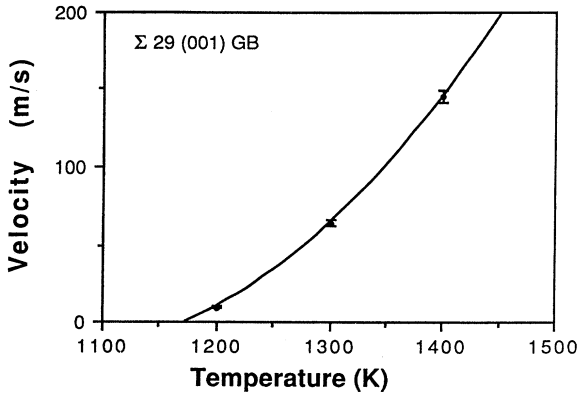

FIG. 9. Velocity of melting for GB-nucleated melting as a function of temperature and extrapolation to zero velocity. The error bars are twice the standard deviation of a fit of $N_{\rm def}$ to a linear function of time.

ting by one interplanar spacing. Under these assumptions, the velocity of propagation at a given temperature $v(T)$ of one liquid-solid interface is given by

$$v(T)=(d_0/58)\partial N_{\rm def}(t,T)/\partial t\ , \tag{21}$$

where d_0 is the interplanar spacing. The velocity of propagation at various temperatures is shown in Fig. 9 where the error bars were taken to be twice the standard deviation in the fit of $N_{\rm def}$ to a linear function of time. The values of the velocity of propagation at various temperatures are given in Table IV. A quadratic extrapolation to zero velocity of propagation yields a temperature of 1179±20 K—in striking agreement with the thermodynamic melting point ($T_m=1171\pm30$ K). The obvious conclusion is that thermodynamic melting has been nucleated at the GB.

VI. FREE-SURFACE NUCLEATED MELTING

A. Free-surface geometry

As discussed in the Introduction and in Sec. IV, the superheating limit for an ideal crystal varies, in practice, with the geometry of the simulation cell. In order to avoid any such effects which might invalidate the comparison of the free-surface and the GB results, we have chosen to use a free-surface geometry as similar as possible to the GB geometry. Specifically, the free-surface (i.e., thin-slab) geometry has the same planar unit cell, the same number of lattice planes, and, consequently, the same number of atoms as the GB geometry. Because there is no (internal) interface, this system consists of an ideal crystal with free (001) surfaces in the z directions.

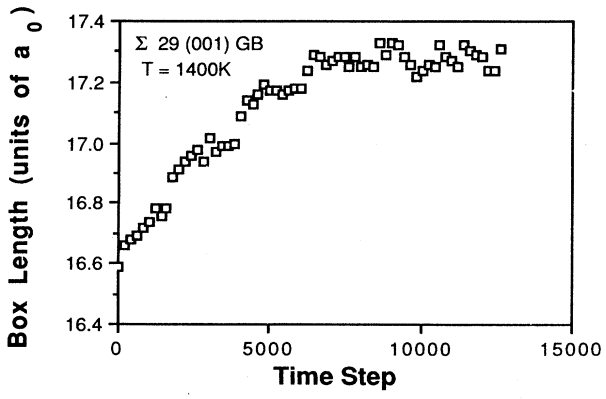

FIG. 8. Length of the bicrystal computational cell in the z direction (parallel to the GB-plane normal) as a function of time at 1400 K. The length of the cell at $T=0$ K is $16.08a_0$. The length for a liquid at 1400 K is $17.31a_0$.

B. Simulation results

Analogous to the GB, the present system is stable at 1100 K. Shown in Figs. 10(a) and 10(b) are the planar structure-factor profiles after 5000 and 10 000 time steps, respectively, at 1300 K. Again, it is seen that a region of disorder nucleates at the site of the defect (i.e., at the surfaces), and spreads throughout the system as time progresses. An examination of the MSD averaged over several planes in the disordered regions yields a diffusion constant which is comparable to that found in the GB simulations. This again indicates that melting has nucleated at the defect and, once having nucleated, spreads throughout the system. Unlike the GB simulation, in which the position of the rigid blocks in region II defined the length of region I in the z direction, there is not a well-defined volume. We are therefore unable to compare the volume expansion with that expected when the system melts.

Figure 11 shows the number of defected atoms as a function of time at both 1300 and 1400 K. An interesting difference from the GB results is the long nucleation time

TABLE IV. Velocity of melting for the GB, $v_{\rm GB}$, the free surface, $v_{\rm FS}$, and the void, v_v, as functions of temperature.

Temperature (K)	$v_{\rm GB}$	$v_{\rm FS}$	v_v
1200	9.67		12.4
1300	63.8	60.4	62.5
1400	145.7	141.0	138.2

(about 5000 time steps) before melting begins at 1300 K. We believe that this is due to the larger amount of intrinsic disorder present in the GB than in the free surface. While the free surface does undergo some small relaxation at zero temperature, its planar structure factor is virtually unity while the planar structure factor in the GB shows considerable disorder even at zero temperature. Therefore, it is reasonable to speculate that the rate of nucleation of melting at a defect depends on the amount of structural disorder present in the defect. Because of the long nucleation time near T_m, no attempt was made to obtain data at 1200 K.

Under the same assumptions as were made in the preceding section, a rate of growth of the disordered region may once again be extracted. In the present case only the data for which $N_{\text{def}} < 100$ were used. The lower limit is necessary to avoid the data during the time of nucleation. As the liquid-solid interfaces approach one another, the free surfaces appear to attract each other as evidenced by the rapid increase in the rate of growth towards the end of the 1400-K simulation (see Fig. 11). The linear behavior prior to the onset of this interaction indicates that the surfaces do not interact substantially. Therefore, in analogy to the GB analysis, we also exclude data for which $N_{\text{def}} > 600$. Altogether, the range

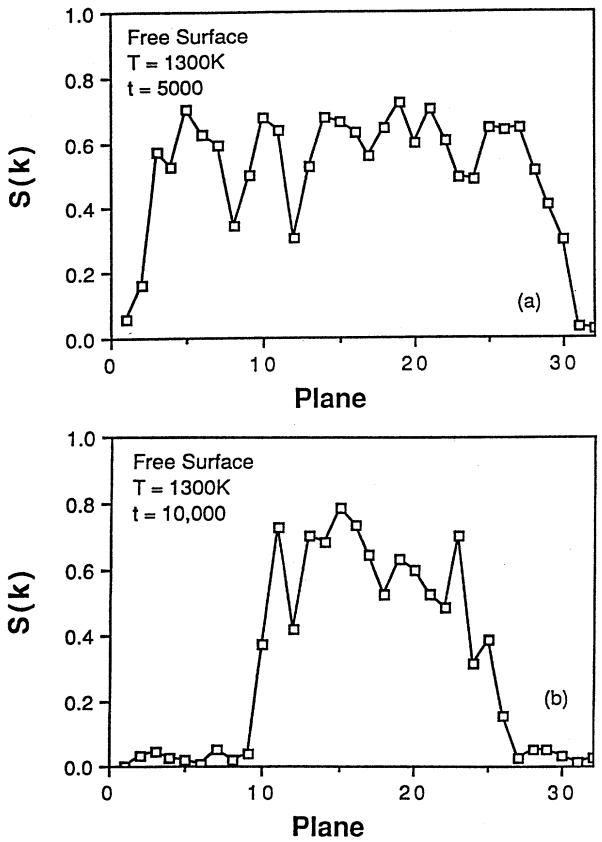

FIG. 10. Instantaneous values of $S_P^2(\mathbf{k}_1)$ and $S_P^2(\mathbf{k}_2)$ for the 32 slices parallel to the (001) free surfaces after 5000 [panel (a)] and 10 000 [panel (b)] time steps at 1300 K.

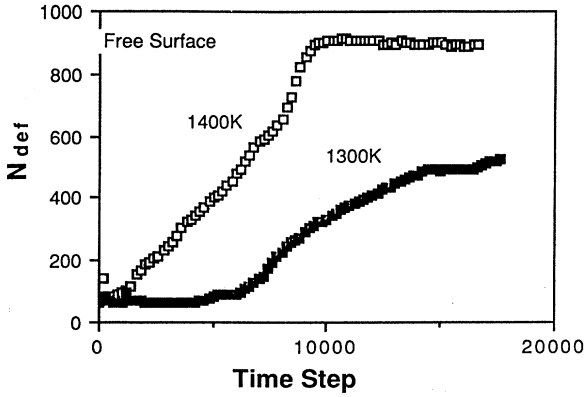

FIG. 11. Number of defected atoms as a function of time for the free surfaces at 1300 and 1400 K.

$100 < N_{\text{def}} < 600$ allows for the melting of more than 17 planes. The velocities obtained are not very sensitive to the precise limits chosen. Shown in Fig. 12 is the rate of growth as a function of temperature for the free surface; the values are listed in Table IV. Extrapolating the two points yields a limiting temperature at which the solid-liquid interface does not propagate (i.e., temperature of coexistence) of 1217±30 K, which is in fairly close agreement with T_m as determined from the free-energy analysis. It is worth noting that without the point at 1200 K, the GB would give a coexistence temperature of 1222 K which is equally high.

VII. VOID-NUCLEATED MELTING

A. Void geometry

To generate a void, we begin with the same ideal-crystal orientation as in the case of the free surface. As discussed in Sec. IV, the region I–region II geometry is used in the present case so as to simulate a planar array of voids. A planar array of one-atom voids (i.e., monova-

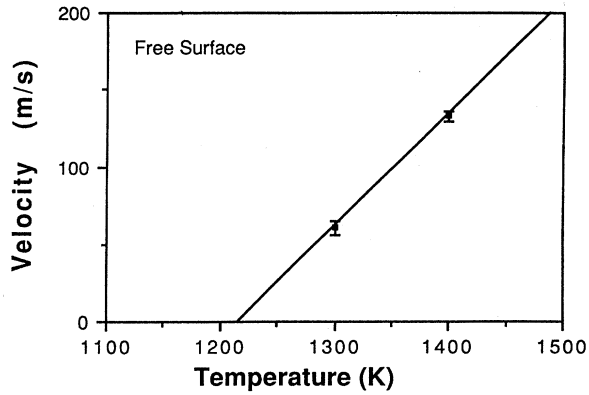

FIG. 12. Velocity of melting for free-surface nucleated melting as a function of temperature and extrapolation to zero velocity. The error bars are twice the standard deviation of a fit of N_{def} to a linear function of time.

cancies) is created be removing a single atom from the center of region I. An array of five-atom planar voids is created by removing a single atom from the center of region I as well as its four nearest neighbors in the (001) (x-y) plane. An array of 13-atom voids is created by removing an atom from the middle of region I as well as all of its twelve nearest neighbors. We note that in the latter two cases, the radii of the voids are between the nearest-neighbor distance, $0.707a_0$, and the second-nearest neighbor distance, $1a_0$, depending on the definition used. Taking the largest value for the radius, and given the planar dimensions of the simulation cell, we find that the distance of the edge of a void from the edge of one of its periodic images is about $1.8a_0$. This is outside the cutoff of the potential so the voids and their images do not interact directly. However, there is an indirect interaction due to interactions between atoms near the void and atoms near its image.

B. Simulation results

No melting was observed in the simulations of a one-atom (monovacancy) void even at 1400 K. In view of the discussion in the preceding section concerning the role of localized disorder in nucleating melting, it is not surprising that the introduction of a single vacancy had no effect. The same was true of the five-atom void where, again, very little disorder was introduced by the defect. This is illustrated in Fig. 13 which shows the profile of the planar structure factor after equilibration at 1100 K. The figure shows that the local planar structure is practically unaffected by the void.

A close examination of the number of atoms per plane shows that during the equilibration at 600 K two atoms from plane 15 "drop" into plane 16 where the five-atom void was initially located; i.e., the void becomes unstable. As the temperature is raised, the void continues to dissociate until it is finally replaced by five highly mobile single-atom vacancies. As in the case of a single vacancy, there is apparently not enough localized disorder to nucleate melting even at 1400 K.

In contrast, the 13-atom void is stable at temperatures below T_m and does nucleate melting above T_m. This is illustrated by Figs. 14(a) and 14(b) showing the profile of the planar structure factor after 5000 and 10 000 time steps, respectively, at 1300 K. The MSD in the disordered region and the overall volume expansion produced by the disordering once again confirm that the system is indeed melting.

The process of melting is initially very different when nucleated by the void than in the case of GB-nucleated or free-surface nucleated melting since the liquid-solid interface now propagates in the x, y, and z directions. However, since the simulation cell is relatively small in the x-y plane, the complete melting of the plane appears to occur rapidly. Nonetheless, it is interesting to compare Figs. 14(a) and 14(b) with the corresponding structure-factor profiles when the melting is nucleated at a GB [Figs. 4(a) and 4(b)]. It is apparent that the transition from the liquid region to the solid region is more gradual in the present case; i.e., the width of the liquid-solid interface appears to be greater. This is consistent with a nonplanar liquid-solid interface as might be expected from the nonplanar nature of the initial defect.

Shown in Fig. 15 is the number of defected atoms as a function of time for melting nucleated by the 13-atom void at 1200, 1300, and 1400 K. If we approximate the liquid-solid interface as being planar, the velocity of melting can be extracted as in the case of the grain boundary. The velocities obtained are listed in Table IV. Figure 16

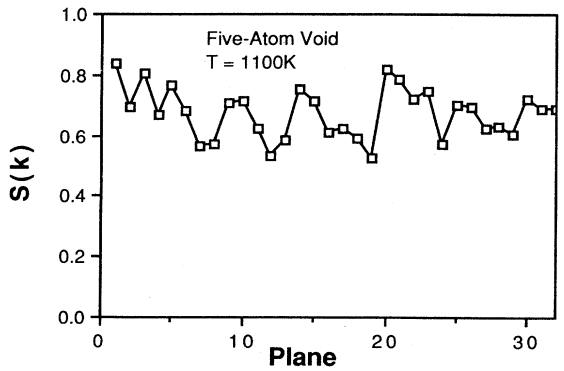

FIG. 13. Instantaneous value of $S_{\hat{p}}^2(\mathbf{k})$ for the 32 slices parallel to the array of five-atom planar voids in the (001) plane after 10 000 time steps at 1100 K.

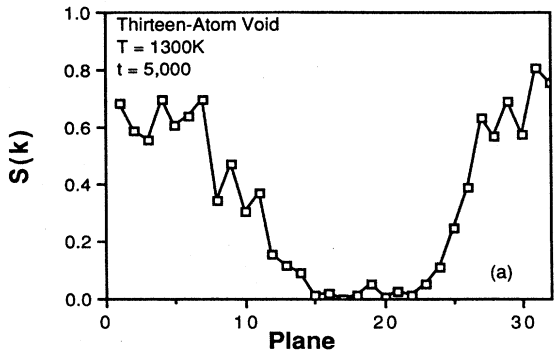

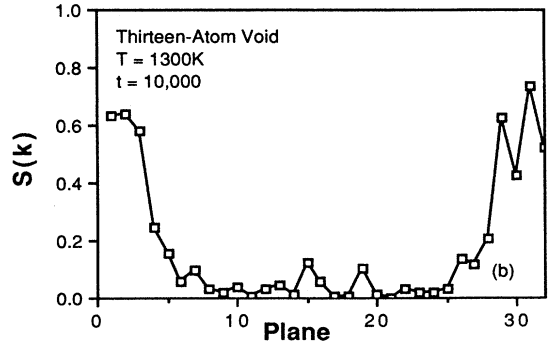

FIG. 14. Instantaneous values of $S_{\hat{p}}^2(\mathbf{k})$ for the 32 slices parallel to the array of 13-atom voids in the (001) plane after 5 000 [panel (a)] and 10 000 [panel (b)] time steps at 1300 K.

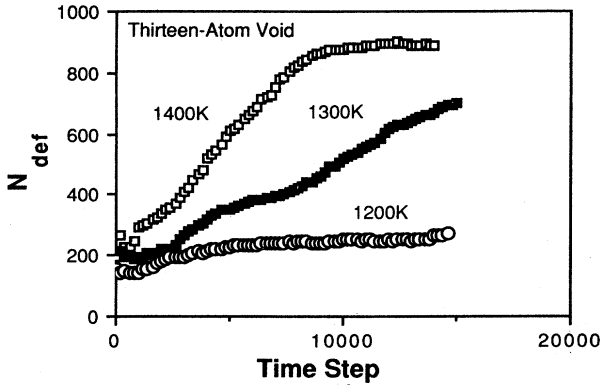

FIG. 15. Number of defected atoms as a function of time for the 13-atom void at 1200, 1300, and 1400 K.

shows the velocity of melting as a function of temperature as well as an extrapolation to zero velocity. The temperature at which no propagation occurs is found to be 1171 ± 20 K which is again very close to T_m.

VIII. DISCUSSION

In this paper, we have presented the results of a molecular-dynamics study on the role of extrinsic defects in the melting process. We have shown that grain boundaries, free surfaces, and voids can act as nucleation sites for melting. By extrapolating the rate of spreading of the melted region away from the nucleation site to zero rate of growth, we found that the defects nucleate melting at all temperatures above T_m and that no melting occurs below T_m. From these results, we draw the following conclusions regarding melting and superheating in real systems.

First, it appears that extrinsic defects are the dominant mechanism for the initiation of melting. This conclusion follows from the fact that MD probes the shortest time scales present in the system simulated. Because an ideal crystal of almost 1000 atoms, simulated with 2D PBC's, remains stable above T_m, thermally generated defects do not appear to cause melting on as short a time scale as do extrinsic defects. Therefore, in any system containing, say, a grain boundary, melting will nucleate at the GB long before any instability due to intrinsic defects takes effect. As was discussed in the Introduction, this observation is in accord with experiment.

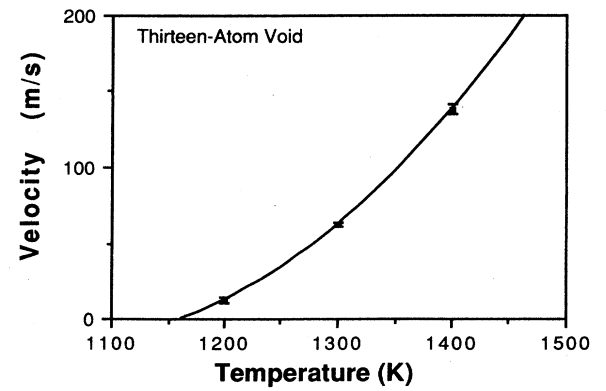

FIG. 16. Velocity of melting for the 13-atom void-nucleated melting as a function of temperature and extrapolation to zero velocity. The error bars are twice the standard deviation of a fit of $N_{\rm def}$ to a linear function of time.

Our second conclusion is that nucleation requires *localized* disorder. This is indicated by the long nucleation times at a free surface as well as the absence of melting when a single vacancy or five-atom void is present. Again, this suggests that intrinsic defects are an unlikely source of melting. Indeed, it is interesting to note that even the five-atom void, which did not nucleate melting, represents a defect concentration of about 0.5% which is substantially higher than the 0.37% called for in theories of melting based on thermally generated defects (see, for example, Ref. 4). We also note that it does not appear that melting requires the presence of an extended defect. Although the 13-atom void does interact indirectly with its periodic images, thus creating a kind of extended defect, the same is true of the five-atom void. Since the latter did not give rise to melting, it appears that the dominant consideration is the amount of disorder present and not the extent of the defect.

We can also identify the mechanical instability which causes spontaneous melting of the ideal crystal at about 1450 K as being that described by the Born criterion. Specifically, Born observed[18] that an fcc crystal becomes unstable when a certain pair of its elastic constants are equal (i.e., when $C_{11}=C_{12}$) and that this occurs when the crystal is sufficiently expanded. We have calculated the elastic constants of our system at zero temperature as a function of lattice expansion and find the instability to occur at an expansion of 4.3%. Although this is only a (quasiharmonic) approximation to the finite-temperature elastic constants, it is interesting to note that at 1450 K, the thermal expansion of the ideal crystal is 3.3%. Since the Born criterion provides an absolute upper limit, and since the elastic-constant calculation is only approximate, we consider these numbers to be remarkably close. This leads us to identify the mechanical instability which limits the degree of superheating one can achieve as arising from this elastic instability. Physically, Young's modulii are zero at this point indicating an instability against variations in the lattice parameter.

The only defect that we have studied extensively below the melting point is the GB. Its behavior below T_m has been discussed in detail elsewhere.[30] Here we only note that the GB appears to be stable below the melting point, in accord with our previous studies using a central-force potential[39] and with experiment.[33–35] This agreement between simulation and experiment concerning the behavior of GB's both below and above T_m indicates that the high-temperature behavior of metal GB's can be reliably investigated by simulation using the currently available techniques.

Finally, the conclusions obtained from the present work are in full agreement with those of paper I which discuss a similar study of melting in silicon. Our results therefore appear to be independent of the nature of bond-

ing. Since the same simulation methods, including the border condition,[51] were used we believe in the broad applicability of this simulation technique to bicrystals.

ACKNOWLEDGMENTS

The authors wish to extend their thanks to H. Gleiter for several useful discussions. In addition, we acknowledge a grant of computer time at the Energy Research Cray XMP at the Magnetic Fusion Research Center at Livermore. This work was supported by the U.S. Department of Energy, Office of Basic Energy Sciences, Materials Science, under Contract No. W-31-109-Eng-38.

APPENDIX

The free energy of a harmonic system is given by[18]

$$G_{\rm har}(T,P=0)=-k_BT\ln(mV^{2/3}k_BT/2\pi h^2)+k_BT\sum_n \ln(h\omega_n/k_BT)+\phi_0 , \quad \text{(A1)}$$

where V is the volume of the system, h is Planck's constant, ϕ_0 is the energy of the static lattice, and $\{\omega_n\}$ is the set of vibrational frequencies of the lattice. The sum in Eq. (A1) extends over $3N-3$ degrees of freedom since it does not include the three zero frequencies associated with center-of-mass motion. The first term on the right-hand side in Eq. (A1) is the contribution of the center of mass. In applying this expression to the reference harmonic solid in the free-energy analysis of Sec. III, the center-of-mass contribution is dropped since the MD system has a fixed center of mass.

The (Helmholtz) free energy of an ideal gas is given by[50]

$$A_i(T,P=0)=k_BT[\ln(n\lambda_T^3)-1] , \quad \text{(A2)}$$

where n is the number density; the de Broglie wavelength is given by

$$\lambda_T^2=2\pi h^2/mk_BT , \quad \text{(A3)}$$

where m is the mass of an atom. Again, the simulations do not allow for center-of-mass motion. Therefore, in using Eqs. (A2)–(A3) in the free-energy analysis, the degrees of freedom associated with the center of mass must be eliminated. In the present case, this is accomplished by evaluating Eqs. (A2)–(A3) for $N-1$ particles.[43] Explicitly, we then have

$$a_i(T,V,N)=1/NA_i(T,V,N-1) . \quad \text{(A4)}$$

*Permanent address: Department of Nuclear Engineering, Massachusetts Institute of Technology, Cambridge, MA 02139.
[1]A. R. Ubbelohde, *Molten State of Matter: Melting and Crystal Structure* (Wiley, Chichester, 1978).
[2]L. L. Boyer, Phase Transition **5**, 1 (1985).
[3]R. M. J. Cotterill, J. Cryst. Growth **48**, 582 (1980).
[4]R. W. Cahn, Nature **273**, 491 (1978).
[5]R. W. Cahn, Nature **323**, 668 (1986).
[6]N. G. Ainslie, J. D. Mackenzie, and D. Turnbull, J. Phys. Chem. **65**, 1718 (1961).
[7]R. L. Cormia, J. D. Mackenzie, and D. Turnbull, J. Appl. Phys. **34**, 2239 (1963).
[8]Ph. Buffat and J.-P. Borel, Phys. Rev. A **13**, 2287 (1976).
[9]J. B. Boyce and M. Stutzmann, Phys. Rev. Lett. **54**, 562 (1985).
[10]C. J. Rossouw and S. E. Donnelly, Phys. Rev. Lett. **55**, 2960 (1985).
[11]J. Daeges, H. Gleiter, and J. H. Perepezko, Phys. Rev. Lett. A **119**, 79 (1986).
[12]See, for example, *Simulations of Liquids and Solids,* edited by G. Ciccotti, D. Frenkel, and I. R. McDonald (North-Holland, Amsterdam, 1987); *Molecular Dynamics Simulation of Statistical Mechanical Systems,* edited by G. Ciccotti and W. G. Hoover (North-Holland, Amsterdam, 1985).
[13]*Monte Carlo Methods in Statistical Physics,* edited by K. Binder (Springer-Verlag, Berlin, 1979).
[14]J.-P. Hansen and L. Verlet, Phys. Rev. **184**, 151 (1969).
[15]J. Q. Broughton and X. P. Li, Phys. Rev. B **35**, 9120 (1987).
[16]D. Frenkel and J. P. McTague, Ann. Rev. Phys. Chem. **31**, 491 (1980).
[17]J. Q. Broughton, G. H. Gilmer, and J. D. Weeks, Phys. Rev. B **25**, 4651 (1982); S. Nosé and F. Yonezawa, Solid State Commun. **56**, 1009 (1985); J. Chem. Phys. **84**, 1803 (1986).
[18]M. Born and K. Huang, *Dynamical Theory of Crystal Lattices* (Oxford, London, 1962).
[19]M. S. Daw and M. I. Baskes, Phys. Rev. Lett. **50**, 1285 (1983), Phys. Rev. B **29**, 6443 (1984).
[20]M. W. Finnis and J. E. Sinclair, Philos. Mag. A **50**, 45 (1984); see also M. Manninen, Phys. Rev. B **34**, 8486 (1986), K. W. Jacobson, J. K. Norskov, and M. J. Puska, *ibid.* **35**, 7423 (1987).
[21]R. Taylor, in *Interatomic Potentials and Crystalline Defect,* edited by J. K. Lee (Metallic Society AIME, Warrendale, PA, 1981).
[22]D. J. Oh and R. A. Johnson, J. Mater. Res. **3**, 471 (1988).
[23]N. W. Ashcroft and N. D. Mermin, *Solid State Physics* (Saunders College, Philadelphia, 1976).
[24]S. M. Foiles, M. I. Baskes, and M. S. Daw, Phys. Rev. B **33**, 7983 (1986); G. J. Ackland, G. Tichy, V. Vitek, and M. W. Finnis, Philos. Mag. **56**, 735 (1987).
[25]M. S. Daw, Surf. Sci. Lett. **166**, L161 (1986); T. E. Felter, S. M. Foiles, M. S. Daw, and R. H. Stulen, *ibid.* **171**, L379 (1986); S. M. Foiles, Surf. Sci. **191**, L779 (1987); M. S. Daw and S. M. Foiles, Phys. Rev. B **35**, 2128 (1987).
[26]W. Moritz and D. Wolf, Surf. Sci. **163**, L655 (1985); M. Copel and T. Gustafsson, Phys. Rev. Lett. **57**, 723 (1987).
[27]D. Wolf, Acta Metall. (to be published).
[28]D. Wolf, Acta Metall. (to be published).
[29]D. Wolf and J. F. Lutsko, Phys. Rev. Lett. **60**, 1170 (1988).
[30]J. F. Lutsko and D. Wolf, Scripta Metall. **22**, 1923 (1989).
[31]S. R. Phillpot, J. F. Lutsko, D. Wolf, and S. Yip, the preceding paper, Phys. Rev. B **40**, 2831 (1989).
[32]K. T. Aust, in *Progress in Materials Science, Chalmers Volume,* edited by J. W. Christian, P. Haasen, and T. B. Massalksi (Pergamon, Oxford, 1981), p. 27; T. Watanabe, S. I.

Kimura, and S. Karashima, Philos. Mag. **49**, 845 (1984).
[33]S. W. Chan, J. L. Liu, and R. W. Balluffi, Scr. Metall. **19**, 1251 (1985).
[34]R. W. Balluffi and R. Maurer, Scr. Metall. **22**, 709 (1988).
[35]R. W. Balluffi and T. S. Hsieh, J. Phys. (Paris) Colloq. **49**, C5-337 (1988).
[36]G. Ciccotti, M. Guillope, and V. Pontikis, Phys. Rev. B **27**, 5576 (1983); M. Guillope, G. Ciccotti, and V. Pontikis, Surf. Sci. **144**, 67 (1984).
[37]P. S. Ho, T. Kwok, T. Nguyen, C. Nitta, and S. Yip, Scripta Metall. **19**, 993 (1985); T. Nguyen, P. S. Ho, T. Kwok, C. Nitta, and S. Yip, Phys. Rev. Lett. **57**, 1919 (1986).
[38]P. Deymier and G. Kalonji, Trans. Jpn. Inst. Met. Suppl. **27**, 171 (1986).
[39]J. F. Lutsko and D. Wolf (unpublished).
[40]S. R. Phillpot, J. F. Lutsko, and D. Wolf, Solid State Commun. **70**, 265 (1989).
[41]J. W. M. Frenken, P. M. Maree, and J. F. van der Veen, Phys. Rev. B **34**, 7506 (1986).
[42]R. Lipowsky and W. Speth, Phys. Rev. B **28**, 3983 (1983).
[43]J. Q. Broughton and G. H. Gilmer, J. Chem. Phys. **79**, 5095 (1983).
[44]F. F. Abraham and J. Q. Broughton, Phys. Rev. Lett. **56**, 734 (1986).
[45]P. Stoltze, J. K. Norskov, and U. Landman, Phys. Rev. Lett. **61**, 440 (1988).
[46]M. D. Kluge and J. R. Ray, Phys. Rev. B **39**, 1738 (1989).
[47]S. Nosé and M. L. Klein, Phys. Rev. Lett. **50**, 1207 (1983).
[48]M. Parrinello and A. Rahman, J. Appl. Phys. **52**, 7182 (1981).
[49]H. C. Andersen, J. Chem. Phys. **72**, 2384 (1980).
[50]L. E. Reichl, *A Modern Course in Statistical Mechanics* (University of Texas Press, Austin, 1980).
[51]J. F. Lutsko, D. Wolf, S. Yip, S. R. Phillpot, and T. Nguyen, Phys. Rev. B **38**, 11 572 (1988).
[52]D. Wolf, J. Phys. (Paris) Colloq. **46**, C4-197 (1985).